J. Fluid Mech. (2007), *vol.* 591, *pp.* 117–144.
doi:10.1017/S002211200700780X Printed in the United Kingdom

The effect of mass ratio and tether length on the flow around a tethered cylinder

K. RYAN, M. C. THOMPSON AND K. HOURIGAN

Fluids Laboratory for Aeronautical and Industrial Research (FLAIR), Department of Mechanical Engineering, Monash University, Melbourne, Victoria 3800, Australia

(Received 18 September 2006 and in revised form 6 June 2007)

A tethered cylinder may be considered an extension of the widely studied problem of a hydro-elastically mounted cylinder. Here we numerically investigate the flow past a positively buoyant tethered cylinder for a range of mass ratios and tether length ratios at a Reynolds number $Re = 200$. The results are found to be qualitatively similar to related experimental work performed at significantly higher Reynolds numbers. Two important findings are related in this paper. First, we find that the action of the tethered cylinder oscillating at an angle to the flow induces a mean lift coefficient. Second, a critical mass ratio (m^*_{crit}) is found below which large-amplitude oscillations are noted, similar to that previously reported for the case of a hydro-elastically mounted cylinder. For short tether lengths, m^*_{crit} is significantly greater than that found for a hydro-elastically mounted cylinder. As the tether length increases, the m^*_{crit} decreases and asymptotes to that of a hydro-elastically mounted cylinder as the tether length approaches infinity.

1. Introduction

Vortex-induced vibration of cylinders is a field that has received considerable study over many years, due largely to its application in mechanical and civil engineering. Several examples highlighting the practical importance of vortex-induced vibration include bridge design, the flow past heat exchanger tubes and the flow past sub-sea riser tubes, used primarily in the oil industry. This interest has motivated numerous fundamental studies. As a result, several comprehensive reviews exist on the topic: for example Sarpkaya (1979), Griffin & Ramberg (1982), Bearman (1984), Parkinson (1989) and Williamson & Govardhan (2004); and the books by Blevins (1990) and Naudascher & Rockwell (1994). In the present study, we focus our attention on the flow past a positively buoyant, tethered cylinder immersed in a uniform flow field with the axis of the cylinder constrained to remain horizontal. The cylinder is constrained to oscillate along the path of an arc of normalized radius $L^* = L/D$, where L is the tether length and D is the cylinder diameter (see figure 1). The study of a tethered cylinder extends the scope of vortex-induced vibrations beyond what has been traditionally considered, as it inherently allows the existence of two new features that have received comparatively little attention to date. The first is that the cylinder oscillation has an imposed curvature (κ) on its path, which is inversely proportional to the tether length; the second is that the cylinder is generally oscillating at a time-averaged mean angle, $\overline{\theta}$, to the free stream. Here $\overline{\theta}$ is imposed by the mean fluid forces acting on the cylinder and may be determined using a simple force balance. This paper aims to investigate the effect that both these features have on the cylinder

oscillation response, and relate the findings to existing results of flow interaction with hydro-elastically mounted cylinders.

To the authors' knowledge, only a few recent publications exist that report investigations on the flow interaction with a buoyant tethered cylinder (for example Ryan *et al.* (2004*a*), Ryan, Thompson & Hourigan (2004*b*) and Browne *et al.* (2005)). Here, we define the tethered cylinder as shown in figure 1. Note, we will not consider the flow past a cylinder tethered solely at one end of the span. Ryan *et al.* (2004*a*) numerically simulated the flow interaction with a tethered cylinder, with a mass ratio $m^*(=\rho/\rho_w)=0.8$, where ρ is the density of the body and ρ_w is the density of the fluid, and $L^*=5$, at a fixed Reynolds number ($Re=\rho u D/\mu=200$). They identified three modes of oscillation, each mode being dependent on the mean layover angle. They referred to these modes as the 'in-line' mode, where oscillations are predominantly in line with the free stream; the 'transverse' mode, where oscillations are predominantly transverse to the free stream; and the 'transition' mode which occurred for mean layover angles between the in-line and transverse modes. They found that oscillations in the transverse mode were similar to those of a low mass-damped, hydro-elastically mounted cylinder held free to oscillate in a direction transverse to the free stream, for which considerable study has been undertaken.

Ryan *et al.*'s (2004*a*) study was extended by Ryan *et al.* (2004*b*), who reanalysed the same results. Ryan *et al.* (2004*b*) observed a negative mean lift coefficient for a majority of mean layover angles considered. The mean lift coefficient only approached zero as $\overline{\theta}\rightarrow 0^\circ$ or 90°. The minimum $\overline{C_L}$ recorded was approximately -0.05, corresponding to $\overline{\theta}\simeq 40^\circ$. They related the non-zero mean lift coefficient to an asymmetry in the wake behind the cylinder. Furthermore, they related the wake asymmetry with the mean layover angle about which the cylinder oscillates, noting that the asymmetry (and hence the magnitude of $\overline{C_L}$) was most prominent in the transition mode.

Recently, Carberry & Sheridan (2007) experimentally investigated the flow interaction with a tethered cylinder for mass ratios in the range $m^*=[0.54, 0.98]$, for a fixed tether length ($L^*=4.6$), and $Re\in[900, 7390]$. They found a mass ratio, ($m^*=0.72$), below which large-amplitude oscillations were observed at high mean layover angles. When the results were plotted against the Froude number ($Fr=u/\sqrt{gD}$, where u is the free-stream velocity and g is the acceleration due to gravity), they found that the jump in amplitude occurred as $Fr\rightarrow 1$ for all $m^*<0.72$. This finding was qualitatively in agreement with the low-Reynolds-number ($Re=200$) numerical findings of Ryan (2004), who determined a mass ratio $m^*=0.38$ below which large-amplitude oscillations were observed. Due to their experimental setup, Carberry & Sheridan (2007) could not determine a negative mean lift, and assumed, for their force balance calculations, that it was negligible compared with the other mean forces acting on the cylinder. This assumption resulted in minor qualitative variations when comparing their experimental findings with the numerical investigations of Ryan (2004).

Within the broader field of vortex-induced vibration, a significant amount of research has focused on hydro-elastically mounted cylinders usually restricted to vibrate only in the direction transverse to the free stream. This arrangement has been chosen as transverse oscillations may be up to an order of magnitude greater in amplitude than oscillations which are in line with the free stream, as shown by Bearman (1984). Classical research in this field has found that, as the frequency of oscillation, f, approaches the natural frequency of the cylinder, f_n, large-amplitude oscillations occur, and further that a narrow range of oscillation frequencies exists where the shedding frequency corresponds to the natural frequency

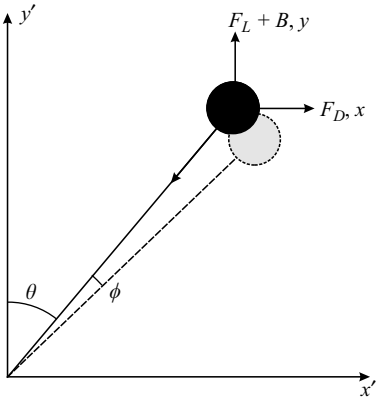

FIGURE 1. Tethered cylinder geometry and coordinate system.

of the cylinder (referred to as the 'lock-in' regime). Large-amplitude oscillations are generally observed within the lock-in regime.

Recent research in this field (notably the work by Khalak & Williamson 1999, Govardhan & Williamson 2000 and Govardhan & Williamson 2003), has focused on the interaction of a low mass-damped hydro-elastically mounted cylinder in a uniform free stream. Khalak & Williamson (1999) found three oscillation 'branches' within the lock-in regime: the 'initial', 'upper' and 'lower' branches. Notably, they found that the 'upper' branch of oscillation exhibited large-amplitude oscillations. Further, they found that the range of reduced velocities ($u^* = u/f_n D$) at which the 'upper' branch was observed varied inversely with mass ratio. Govardhan & Williamson (2000) determined a critical mass ratio, m^*_{crit}, below which the lower branch should not be found. Instead, large-amplitude oscillations, in the upper branch, were observed, and it was hypothesized that these large-amplitude oscillations should occur up to and including $u^* = \infty$. For Reynolds numbers in the range $Re = [4000, 22000]$, they determined a critical mass ratio $m^* = 0.54$. Govardhan & Williamson (2003) extended these findings by conducting a study where $u^* = \infty$. In that study, they found large-amplitude oscillations for $m^* < 0.54$, in agreement with the prior study. They also determined a critical mass ratio for a much lower Reynolds number ($Re = 100$), from the numerical results obtained by Shiels, Leonard & Roshko (2001). At this lower Reynolds number, the critical mass ratio was found to be $m^*_{crit} \simeq 0.25$. Recent work by Ryan, Thompson & Hourigan (2005) has extended this finding by determining the critical mass ratio in the Reynolds number range $Re = [40, 200]$. Their findings show a significant variation of m^*_{crit} as a function of Reynolds number, within the low-Reynolds-number range investigated. Extending this finding to the case of a tethered cylinder, the qualitative differences of the critical mass ratio reported by Ryan (2004) and Carberry & Sheridan (2007) are not altogether surprising. Indeed, when the experiments and numerics are compared, the drag, lift and mean layover results are found to have the same form, although the actual quantitative values differ due to the large variation in Reynolds number (see Ryan 2004 for further details).

The similarity of the results for the flow past a tethered cylinder with those found for a low mass-damped, hydro-elastically mounted cylinder raises several interesting questions which this paper aims to answer.

(i) How is the jump in amplitude observed for a tethered cylinder related to the jump observed for a freely oscillating cylinder, and why is there a variation in the critical mass ratio at which this jump occurs between the two systems?

(ii) What is the effect of curvature on the oscillating modes observed for the tethered cylinder? Otherwise stated, what is the effect of varying L^*?

(iii) What is the effect of the mean layover angle, and how does an oscillation at an angle to the free stream alter the wake dynamics when compared to a freely oscillating cylinder?

In order to analyse the results, and to compare the present results with previous findings for a hydro-elastically mounted cylinder, we introduce the equation of motion for a tethered cylinder:

$$J\ddot{\theta} = F_\theta L, \tag{1.1}$$

where J is the polar moment of inertia, F_θ is the force acting on the cylinder in the direction of motion, and L is the tether length. In (1.1), both F_θ and θ have a mean and time-dependent component ($\theta = \overline{\theta} + \theta^t$, $F_\theta = \overline{F}_\theta + F_\theta^t$).†

We can express F_θ as a function of the drag, lift and buoyancy forces acting on the cylinder as

$$F_\theta = F_D \cos(\theta) - (F_L + B)\sin(\theta), \tag{1.2}$$

where F_D and F_L are the drag and lift forces respectively, and B is the buoyancy force, which takes into account the force of gravity. By assuming small-amplitude oscillations, such that $\sin(\theta') \simeq \theta'$ and $\cos(\theta') \simeq 1$, F_θ may be separated into its mean and time-dependent components as

$$F_\theta = -\theta^t(\overline{T} + T^t) + F_{osc}, \tag{1.3}$$

where

$$\overline{T} = \overline{F}_D \sin(\overline{\theta}) + \overline{F}_L \cos(\overline{\theta}), \tag{1.4}$$

$$T^t = F_D^t \sin(\overline{\theta}) + F_L^t \cos(\overline{\theta}), \tag{1.5}$$

$$F_{osc} = \left(F_D^t \cos(\overline{\theta}) - F_L^t \sin(\overline{\theta})\right), \tag{1.6}$$

$\overline{T}$ is the mean tension force acting through the tether and T^t is the time-varying tension force component. Combined they constitute the restoring force of the system, as they are a multiple of θ^t in (1.3). F_{osc} may be considered as the driving force, consisting of the collection of time-varying force components acting in the direction of motion which are not a multiple of θ^t in (1.3).

Substituting this definition of F_θ into (1.1), the equation of motion may be rewritten as follows:

$$J\ddot{\theta} + \theta^t(\overline{T} + T^t)L^*D = F_{osc}L^*D. \tag{1.7}$$

In contrast to the case of a hydro-elastically mounted cylinder, the spring restoring force for a tethered cylinder is dependent on both the mean and time-varying fluid force components acting on the cylinder.

By following the work of Khalak & Williamson (1999) (and references cited therein), we may decompose the forces acting on the cylinder into the inviscid and viscous force components: $F_{osc} = F_{potential} + F_{vort}$. The potential force, $F_{potential}$, is the force which would act on the cylinder in an ideal fluid, and we may determine this force

† In general, for a variable β, we shall define $\overline{\beta}$ as the mean value and β^t as the time-varying component.

component analytically. By making this substitution, the natural frequency of the system within the fluid may be determined.

For the particular case of the tethered cylinder, the rotation of the cylinder, in conjunction with linear displacement, leads to a nonlinear equation describing the inviscid fluid forces acting on the system (see Newman 1977 for further details):

$$F_{potential} = -[\ddot{\theta} L^* D + 2u\dot{\theta}\theta^t \cos\overline{\theta} + 2u\dot{\theta} \sin\overline{\theta}] m_D C_A, \tag{1.8}$$

where m_D is the mass of the fluid displaced by the cylinder, and C_A is the added-mass coefficient within the inviscid fluid. For planar motion, the added-mass coefficient is equal to unity for a cylinder of circular cross-section. For the case of a short tether length, where the cylinder motion has a large curvature, the added mass is no longer unity. This case is equivalent to a cylinder immersed within a sinusoidally oscillating flow, which has been described by Newman (1977) and Lamb (1932).

Substituting this equation into the equation of motion (1.7) and decomposing the fluid force into the inviscid and vortex force components leads to a nonlinear equation describing the motion of the cylinder:

$$(J + L^{*^2} D^2 m_D C_A)\ddot{\theta} + [2u\theta^t \cos\overline{\theta} + 2u \sin\overline{\theta}] m_D C_A L^* D\dot{\theta} + [\overline{T} + T^t] L^* D\theta^t = F_{vort} L^* D. \tag{1.9}$$

A solution to this problem exists in the limit that $L^{*^2} \to \infty$, representing the case where there is no restoring force acting on the system. In this case we approximate the moment of inertia of the system,

$$J = mD^2\left(L^{*^2} + \tfrac{1}{8}\right) \to mD^2 L^{*^2}, \tag{1.10}$$

and we substitute $\xi = \theta^t L^* D$, where ξ is the displacement of the cylinder in the direction of motion; and rewrite (1.9) to form

$$(m + m_D C_A)\ddot{\xi} = F_{vort}. \tag{1.11}$$

This is precisely the equation of motion obtained by Govardhan & Williamson (2003) for the case of a hydro-elastically mounted cylinder with the restriction that $u^* = \infty$; albeit that the direction of motion in the case of the tethered cylinder is dependent on the mean fluid forces acting on the cylinder. It is therefore anticipated that as $L^* \to \infty$, the motion of a tethered cylinder will approach that of a freely oscillating cylinder at $u^* = \infty$. Given the similarity between the two systems, the hydro-elastically mounted cylinder may be considered a special case of the tethered cylinder system. The principal difference between the two systems is that the tethered cylinder, even with a very large tether length, oscillates at an angle to the free stream, where the angle is dependent on the mass ratio of the cylinder and the Froude number of the flow. By contrast, the studies by Govardhan & Williamson (2003) restricted the motion of the cylinder to be normal to the inflow direction.

In § 2 the methodology used in this investigation is described in detail. Section 3.1 describes the response of the tethered cylinder system as the mass ratio is varied. In § 3.2 we consider the response of the tethered cylinder system as the tether length is varied. Finally, in § 3.2.5 we consider the variation of the critical mass ratio as a function of tether length.

2. Problem description and methodology

The coordinate system and geometry of the problem are shown in figure 1. Note that θ is the layover angle formed by the tether and the y-axis, and the tether length

is measured from the tether attachment point to the centre of the cylinder. The forces acting on the cylinder are composed of the drag, lift and buoyancy forces and the tension in the tether. The buoyancy force is combined with the lift force to give a net vertical force (denoted as $F_L + B$ in figure 1).

2.1. *Modelling the flow field*

The numerical technique employed obtains a solution of the two-dimensional, incompressible form of the Navier–Stokes equations, expressed in primitive variable form,

$$\frac{\partial \boldsymbol{u}}{\partial t} + \boldsymbol{u}\cdot\nabla\boldsymbol{u} = -\nabla p + \nu\nabla^2\boldsymbol{u}, \tag{2.1}$$

where p is the kinematic pressure, ν is the kinematic viscosity and $\boldsymbol{u} = (u(t, x, y), v(t, x, y))$ is the two-dimensional velocity vector. Equation (2.1) is coupled with the incompressibility condition,

$$\nabla\cdot\boldsymbol{u} = 0, \tag{2.2}$$

to complete the set. The spatial derivatives are evaluated using a spectral-element discretization technique. The spatial accuracy is determined at run time by choosing the order of the tensor product of interpolating polynomials within each macro-element. In this study ninth-order interpolant polynomials were used within each element, after a rigorous *H-P* refinement analysis was performed. Results of this study are reported in detail in Ryan (2004). For the cases reported herein, the computational grid comprised 518 macro-elements; the inlet was 15 diameters upstream of the leading edge of the cylinder, the outlet was 23 diameters downstream of the trailing edge of the cylinder, and the sidewalls were 30 diameters apart. As the reference frame of the computational grid was attached to the cylinder, these boundary conditions remained constant throughout the computation.

Temporal derivatives were evaluated using a classical three-step splitting scheme, achieving second-order time accuracy. The algorithm employed has been used previously for a variety of flow problems (for example Sheard, Thompson & Hourigan 2003, Hourigan, Thompson & Tan 2001 and Pregnalato 2003) and is described in detail in Thompson, Hourigan & Sheridan (1996) and references cited therein.

2.2. *The governing equations of motion and the coupling technique*

The equations of motion have been determined by relating the instantaneous acceleration of the cylinder to the fluid forces acting on the cylinder. In Cartesian coordinates they are written

$$m\ddot{x} = F_D - T\sin\theta, \tag{2.3}$$

$$m\ddot{y} = (F_L + B) - T\cos\theta. \tag{2.4}$$

Normalizing these equations, we may write

$$\frac{\pi}{2}m^*\ddot{x}^* = C_D\left(\frac{y^{*2}}{L^{*2}}\right) - \left(C_L + \frac{\pi}{2Fr^2}(1-m^*)\right)\frac{x^*y^*}{L^{*2}}, \tag{2.5}$$

$$\frac{\pi}{2}m^*\ddot{y}^* = \left(C_L + \frac{\pi}{2Fr^2}(1-m^*)\right)\frac{x^{*2}}{L^{*2}} - C_D\frac{x^*y^*}{L^{*2}}. \tag{2.6}$$

Here $x^* = x/D$, $y^* = y/D$, are the normalized displacement components and $\ddot{x}^* = \ddot{x}D/u^2$, $\ddot{y}^* = \ddot{y}D/u^2$, are the normalized components of instantaneous acceleration. From the solution of the Navier–Stokes equations, (2.1) and (2.2), at the $(n+1)$st time step, we have estimates of the fluid velocities and pressure field. We then use these to

calculate the fluid forcing coefficients, C_D and C_L, acting on the body at the $(n+1)$st time step. The acceleration of the body is then calculated using (2.5) and (2.6). For each time step, the solution is successively updated using an Adams–Bashforth/Adams–Moulton predictor–corrector technique. Details of the predictor–corrector technique may be found in Ryan (2004).

Note that the Cartesian formulation used for the simulations is based on a point-mass approximation. This means that the approximation given by (1.10) is assumed. This is appropriate provided that the tether lengths chosen for investigation are $L^* \gtrsim 1$. This restriction was the limiting factor in the range of L^* chosen in this investigation.

Inspection of (2.6) reveals that the equations are controlled by selection of m^*, L^* and Fr. As will be detailed in the next section, the Froude number was chosen as the flow-controlling parameter in this study.

2.3. *Definition of the controlling parameter*

Within the broader field of vortex-induced vibration, the reduced velocity is often used as the controlling parameter describing the flow field. The reduced velocity is defined as

$$u^* = \frac{u}{f_n D}, \tag{2.7}$$

where f_n is the natural frequency of the system. For the case of the tethered cylinder, the reduced velocity can only be determined analytically when considering the natural frequency of the system within a vacuum. However, even with this simplification, the dependence of the natural frequency (and hence the reduced velocity) on the drag and lift forces makes the determination of the reduced velocity impossible from knowledge of the static variables and inlet conditions alone. Therefore, we have chosen a 'reduced' Froude number as our controlling parameter, where

$$Fr' = \frac{u}{\sqrt{(gD)(1-m^*)}} = \frac{\text{inertial force}}{\text{buoyancy force}}. \tag{2.8}$$

This parameter was chosen as it allows an excellent collapse of results across mass ratios and tether lengths. For all simulations the Reynolds number, based on the inlet velocity and cylinder diameter, was held constant ($Re = 200$), and the reduced Froude number was varied independently. For comparison with previous studies, the reduced Froude number may be related to the reduced velocity (in a vacuum) through the relation

$$u^* = 2\pi \left[\frac{\pi(m^*)(L^{*2} + 1/8)}{2\left[C_D^2 + (\pi/2Fr'^2 + C_L)^2\right]^{1/2} L^*} \right]^{1/2}. \tag{2.9}$$

3. Results and discussion

3.1. *Variation of mass ratio*

Our initial investigation concerns the analysis of a tethered cylinder with a fixed tether length ($L^* = 5.0$) for various mass ratios ($m^* = [0.1, 0.8]$). This tether length was chosen to agree with previous studies (Ryan *et al.* 2004*a*, 2004*b*). We commence by investigating the variation of the mean layover angle as a function of the reduced Froude number.

3.1.1. *Mean layover angle results*

Figure 2 presents the layover angle results as a function of the reduced Froude number for a range of mass ratios. The results are in qualitative agreement with the

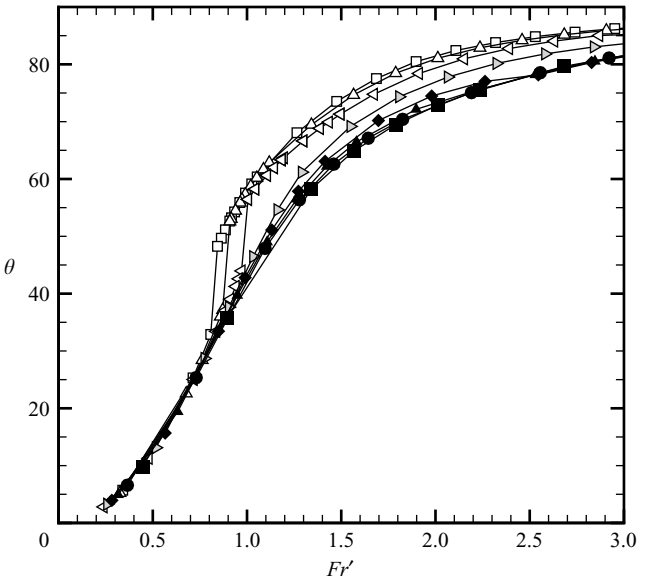

FIGURE 2. Mean layover angle as a function of reduced Froude number, $L^* = 5.0$, $m^* \in [0.1, 0.8]$; □, $m^* = 0.1$; △, $m^* = 0.2$; ◁, $m^* = 0.3$; ▷, $m^* = 0.4$; ◆, $m^* = 0.5$; ▲, $m^* = 0.6$; ● $m^* = 0.7$; ■ $m^* = 0.8$.

experimental findings of Carberry & Sheridan (2007). For $Fr' < 0.8$, all the results collapse onto the same curve, regardless of mass ratio. Two distinct response plots are observed for $Fr' \gtrsim 0.8$. For relatively large mass ratios ($m^* \geqslant 0.4$), the results collapse onto a smoothly varying curve for all Fr' considered. For mass ratios below 0.3, a discontinuous jump is observed at $Fr' \simeq [0.8, 1.0]$. The discontinuity results in an increase in $\overline{\theta}$ of the order 20°. Beyond $Fr' = 1.0$, the results for mass ratios $m^* \leqslant 0.3$ collapse well onto a smooth curve with $\overline{\theta}$ increasing with increasing reduced Froude number.

The case of $m^* = 0.4$ is of particular interest; here a deviation in the mean layover angle away from that of higher m^* cases was noted for $Fr' > 1.2$. However, no discontinuous jump is observed and the results for $m^* = 0.4$ lie between the higher and lower m^* curves at high Fr'.

These findings raise two interesting points. First, the significant jump in $\overline{\theta}$, noted for $m^* \leqslant 0.3$, implies a discontinuous change in the dominant direction of oscillation for these mass ratios. Prior to the discontinuous increase in $\overline{\theta}$, the dominant component of oscillation was in line with the flow field. Beyond the jump, the dominant component of oscillation was found to be transverse to the flow field. Second, from a simple force balance, the mean layover angle can be related to the fluid forces acting on the body, where the relation is given as

$$\overline{\theta} = \tan^{-1}\left(\frac{\overline{C_D}}{\overline{C_L} + \pi/2Fr'^2}\right). \tag{3.1}$$

From the form of (3.1), the discontinuous change in $\overline{\theta}$ is directly linked to either a discontinuous increase in $\overline{C_D}$ and/or a discontinuous decrease in $\overline{C_L}$. Therefore, from this result we predict a discontinuous alteration in the mean forces acting on the

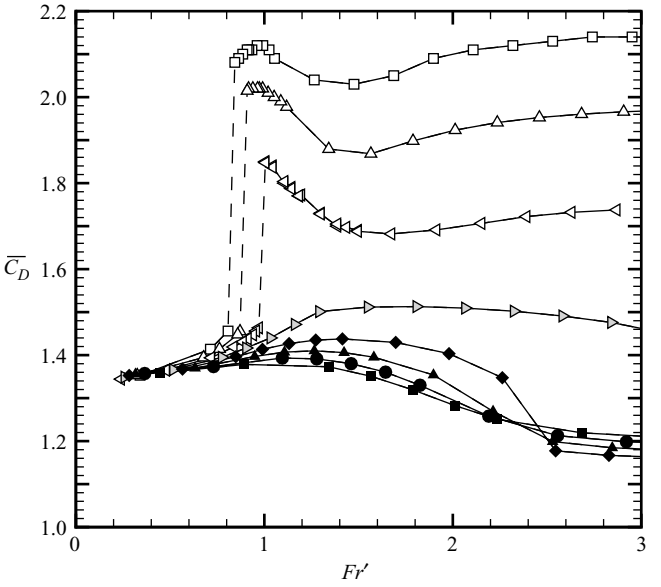

FIGURE 3. Mean drag coefficient as a function of reduced Froude number. $L^* = 5.0$, $m^* \in [0.1, 0.8]$. Symbol definitions are the same as for figure 2.

cylinder (for $m^* \leqslant 0.3$ and $Fr' \geqslant [0.8, 1.0]$), and hence a discontinuous change in the wake state.

3.1.2. *Mean drag coefficient results*

Figure 3 presents the variation of $\overline{C_D}$ as a function of Fr'. As anticipated, a distinct discontinuous jump in $\overline{C_D}$ is noted for $m^* \leqslant 0.3$ as the reduced Froude number increases through the range $Fr' = [0.8, 1.0]$. For higher mass ratios, $\overline{C_D}$ increases continuously for low values of Fr' before gradually decreasing once more. At high values of Fr' ($Fr' \gtrsim 3.0$), the mean drag found for $m^* \geqslant 0.4$ is significantly less than that found for $m^* \leqslant 0.3$.

For high mass ratio cases ($m^* \geqslant 0.5$), the drag reduces to $\overline{C_D} \simeq 1.2$ at high Fr' numbers. Remarkably, this value of $\overline{C_D}$ is smaller than that observed at $Fr' \simeq 0.2$, implying a change in the wake structure interaction at these high Fr' values when compared to low Fr'. This variation is independent of the flow Reynolds number (Re was held constant for all simulations) and it is assumed that it is purely the motion of the cylinder which induces this reduction in drag coefficient. As with the findings for $\overline{\theta}$, the particular case of $m^* = 0.4$ represents an interesting case. While not exhibiting a discontinuous increase in $\overline{C_D}$, the $m^* = 0.4$ case does exhibit appreciably higher drag at relatively high values of Fr' ($Fr' \gtrsim 2$).

For low mass ratios ($m^* \leqslant 0.3$), the increase in $\overline{C_D}$ is significant across the discontinuous jump. The variation in $\overline{C_{D\max}}$ was found to be inversely proportional to the mass ratio, the highest $\overline{C_D}$ found being $\overline{C_D} = 2.12$ for $m^* = 0.1$. In contrast to the high m^* results, for $m^* \leqslant 0.3$ the increase in $\overline{C_D}$ was found to remain significant up to the highest Fr' considered, ($Fr' = 50$). For each of these low m^* cases, the drag observed at $Fr' \simeq 3.0$ remained almost constant for all higher Fr' values considered.

There is a subtle difference in the mean drag response for reduced Froude numbers beyond the discontinuous jump which varies as a function of mass ratio. For the lowest mass ratio case investigated, $m^* = 0.1$, and beyond the discontinuity, the mean

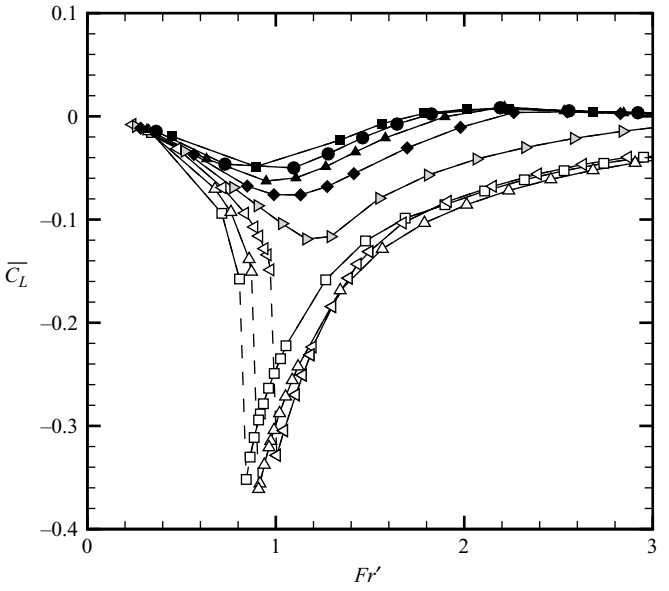

FIGURE 4. Mean lift coefficient as a function of reduced Froude number. $L^* = 5.0$, $m^* = [0.1, 0.8]$. Symbol definitions are the same as for figure 2.

drag increases further in the range $Fr' = [0.8, 1.0]$, before smoothly decreasing. Within the same range, a smaller continuous increase in $\overline{C_D}$ is noted for $m^* = 0.2$; however, no further increase in $\overline{C_D}$ is noted within this range for $m^* = 0.3$. This finding may imply that the mechanism causing the discontinuous increase for the case of $m^* = 0.1$ may be subtly different when compared with higher mass ratio cases. As Fr' increases beyond $Fr' \simeq 1.2$, all mass ratio cases that experienced a discontinuous jump show a further smooth increase in $\overline{C_D}$ up to $Fr' \simeq 3.0$.

3.1.3. *Mean lift coefficient results*

Figure 4 shows the mean lift coefficient as a function of Fr'. A significant variation in $\overline{C_L}$ is observed associated with the jump in $\overline{\theta}$, in agreement with the conclusions in § 3.1.1. Negative values of $\overline{C_L}$ are observed for all mass ratios considered. For mass ratios that do not exhibit a jump in $\overline{\theta}$ ($m^* \geqslant 0.4$), the variation in $\overline{C_L}$ away from the *zero line* is quite small, the largest variation being for $m^* = 0.4$, where a local minimum of $\overline{C_L} \simeq -0.12$ exists at $Fr' \simeq 1.2$. For higher reduced Froude numbers, the lift coefficient for $m^* \geqslant 0.5$ actually increases such that positive lift is observed, with a local maximum at $Fr' \simeq 2.0$. However, this local maximum is negligibly small when compared with the minimum values observed, and $\overline{C_L} \to 0$ for large Fr' for all mass ratios considered.

Mass ratios which exhibit a jump in $\overline{\theta}$ ($m^* \leqslant 0.3$) exhibit a significant decrease in $\overline{C_L}$ at the corresponding Fr' where the jump in $\overline{\theta}$ is observed. For these cases, a sharp local minimum in $\overline{C_L}$ is observed at $Fr' \simeq [0.8, 1.0]$ ($\overline{C_L} \simeq -0.36$ in each case). For higher reduced Froude numbers, the mean lift coefficient smoothly increases once more, approaching $\overline{C_L} = 0$ at high Froude numbers.

The variation in $\overline{C_L}$ is perhaps more surprising than that noted for $\overline{C_D}$; while a finite mean lift has been noted for the case of a forcedly oscillating cylinder (Blackburn & Henderson 1999), this has only been observed for a narrow band of oscillations where P+S shedding was observed. Given the broad range of Fr' over which a finite

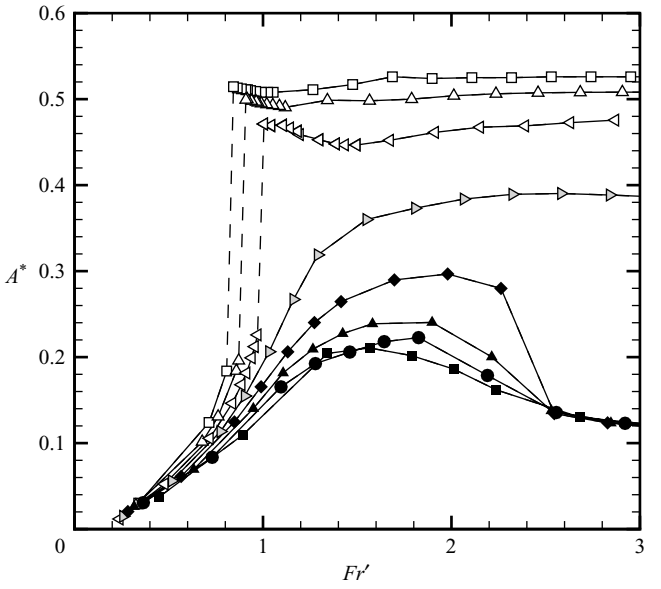

FIGURE 5. Amplitude of oscillation, A^*, as a function of reduced Froude number. $L^* = 5.0$, $m^* = [0.1, 0.8]$. Symbol definitions are the same as for figure 2.

mean lift is observed for the case of a tethered cylinder, it is presumed that a different mechanism is behind the current observations. Three major differences exist between the tethered cylinder and the hydro-elastically mounted cylinder systems. First the tethered cylinder system oscillates at an angle to the free stream; second the tethered cylinder system oscillates along an arc; and third the restoring force for the tethered cylinder system is nonlinearly coupled with the fluid forces acting on the cylinder. Any of these factors could individually or in combination account for the negative $\overline{C_L}$ values observed in figure 4. As will be discussed further in § 3.1.6, the non-negligible $\overline{C_L}$ was found to be directly related to the angle at which the cylinder is oscillating, coupled with the amplitude of oscillation.

The variation in both mean lift and drag indicates a significant change in the wake flow field. In particular, for $m^* \leqslant 0.3$ it is anticipated that the dramatic increase in $\overline{C_D}$ and $|\overline{C_L}|$ is associated with a corresponding discontinuous increase in A^*.

3.1.4. *Amplitude of oscillation results*

Figure 5 shows A^* as a function of Fr'. As predicted, a significant jump in the amplitude is observed for $m^* \leqslant 0.3$, occurring in the reduced Froude number range $Fr' \simeq [0.8, 1.0]$. For lower reduced Froude numbers, the amplitude data collapse reasonably well regardless of mass ratio. For $m^* > 0.4$, a relatively small local maximum in A^* is observed in the range $Fr' \simeq [1.0, 2.0]$. The range of Fr' at which non-negligible oscillations are sustained varies inversely with the cylinder mass ratio. This may be compared with the results of Govardhan & Williamson (2000) who reported similar behaviour when considering the case of the hydro-elastically mounted cylinder.

By contrast, the oscillation amplitude observed for $m^* \leqslant 0.3$ remained significant up to the highest Fr' considered ($Fr'_{\max} = 50$). We found significant amplitudes for $m^* = 0.4$ over a range of reduced Froude numbers. However, at high Fr' the oscillation amplitude for $m^* = 0.4$ approaches $A^* = 0.1$.

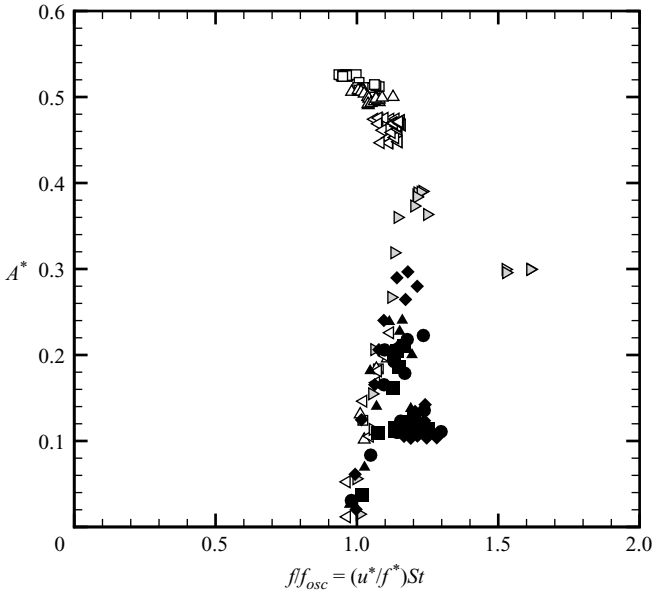

FIGURE 6. Oscillation amplitude, A^* as a function of frequency ratio. $L^* = 5.0$, $m^* = [0.1, 0.8]$. Symbol definitions are the same as for figure 2.

3.1.5. *Comparison with the hydro-elastically mounted cylinder*

So far, the results have indicated the presence of two interesting phenomena. The first is that the mean lift coefficient is negative for a significant part of the parameter space. The second is that a mass ratio exists below which a jump in A^* is observed; this jump occurs within a narrow range of Fr'. For mass ratios that exhibit this discontinuous increase, large-amplitude oscillations are observed for all $Fr' \gtrsim 0.8$ investigated.

It is of interest to examine whether the dramatic increase in amplitude is due to the same phenomena underlying the 'critical mass ratio' observed for the hydro-elastically mounted cylinder. Qualitatively the two phenomena appear to be the same, and we shall refer to the mass ratio at which the jump occurs as the critical mass ratio (m^*_{crit}). Figure 6 shows the amplitude as a function of a frequency ratio ($f/f_{osc} = (u^*/f^*)St$), where f is the shedding frequency for a stationary cylinder at the same Reynolds number, and f_{osc} is the principal oscillation frequency. Our results are qualitatively similar to those found by Govardhan & Williamson (2000) for a low mass-damped hydro-elastically mounted cylinder. It should be noted that beyond the low-amplitude oscillations (where the frequency ratio $f/f_{osc} \simeq 1$), the mean layover angle $\overline{\theta} > 45^\circ$ and the cylinder is oscillating predominantly transverse to the free stream, so the tethered cylinder system should behave similarly to the hydro-elastically mounted cylinder.

For all mass ratios considered, a linear increase in A^* is noted as a function of frequency ratio. Within this range (corresponding to $\overline{\theta} < 45^\circ$), the cylinder is oscillating predominantly in line with the flow. For $m^* \leqslant m^*_{crit}$ a discontinuous increase in A^* is noted (while the frequency ratio remains essentially constant), and for $m^* > m^*_{crit}$ a dramatic reduction in A^* is noted, and the frequency ratio increases. The linear increase in amplitude noted in all cases is reminiscent of the 'initial' branch observed for the hydro-elastically mounted cylinder; the peak value of oscillation is reminiscent of the 'upper branch'; and (for $m^* > m^*_{crit}$) the low-amplitude results are reminiscent

of the 'lower' branch. Based on this qualitative assessment, it is probable that similar mechanisms are at work in both the tethered and hydro-elastically mounted cylinder systems. We therefore conclude that the phenomena are essentially the same in both cases, although the addition of a tether alters the critical mass ratio at which a jump is observed. Prior work by Ryan (2004), and Ryan (2004*b*) has indicated that the critical mass ratio for a hydro-elastically mounted cylinder at $Re = 200$ is $m^*_{crit} \simeq 0.1$. If what we have observed in § 3.1.4 is evidence of the same mechanism, then the tethered cylinder has a significantly higher critical mass ratio for the same Reynolds number. Indeed, Ryan (2004) found the critical mass ratio for the tethered cylinder with $L^* = 5.0$ and $Re = 200$ to be $m^*_{crit} = 0.36$. We will consider the effect of tether length on the critical mass ratio in § 3.2.5.

In the next section, we turn our attention to another phenomenon apparent when comparing the tethered cylinder to the hydro-elastically mounted cylinder, namely the presence of a non-zero mean lift. Section 3.1.6 considers the flow structures in the wake of a tethered cylinder over one cycle of oscillation. The conclusion from this analysis is that the variation in mean lift is due to the combination of the cylinder oscillation and the mean layover angle. This result is confirmed in § 3.2, where we investigate the effect of tether length (effectively changing the radius of curvature of motion). Here, we find that the mean lift is relatively independent of the tether length. Hence, we conclude that it is the layover angle, and not the radius of curvature, which is responsible for the finite mean lift.

3.1.6. *The vortex-shedding process in the wake of a tethered cylinder*

As noted in § 3.1.3, a non-zero mean lift coefficient is observed for a majority of the cases investigated. It should be reiterated that, for both low and very high Froude numbers, the mean lift approaches zero. The finite mean lift is clearly influenced by the angle at which the moving cylinder oscillates with respect to the surrounding fluid. While the wake structures and the cylinder form a coupled system, this section will describe the flow from the perspective of the influence of the cylinder motion on the formation and propagation of flow structures in the wake. It should be remembered that the wake structures continually influence the forces acting on the cylinder and its subsequent motion in a feedback loop.

This section will concentrate on the case of a cylinder oscillating with a high amplitude. Specifically, the vortex-shedding cycle will be investigated for the case of $m^* = 0.1$ and $Fr = 0.8$. The case of low amplitude oscillations has previously been considered by Ryan, Thompson & Hourigan (2004*b*).

Figure 7 shows a snapshot of the vortex structures in the tethered cylinder wake. The cylinder is at the top of its cycle, defined as the most anticlockwise position, and is momentarily stationary. Two related features of the shedding wake distinguish this case from either the flow past a fixed cylinder or past a freely oscillating cylinder. First, the wake is clearly shedding at an angle to the inflow. In itself, this is indicative of the mean negative lift acting on the tethered cylinder. Second, the fluid structures are shed in discrete vortex pairs. These structures induce a jet of fluid to travel in the positive y-direction (relative to the vortex pair) inducing both the mean negative lift and the angle at which the wake is shed. The motion of the cylinder is responsible for inducing the vortex pairing.

Figure 8(*a*) to 8(*d*) show a sequence of close-up snapshots of vorticity in the wake at quarter-cycle intervals. Figure 8(*a*) shows the shedding structures, taken for the case of the cylinder moving midway between the bottom position and the top position of the oscillation cycle. The cylinder is instantaneously moving both upstream and

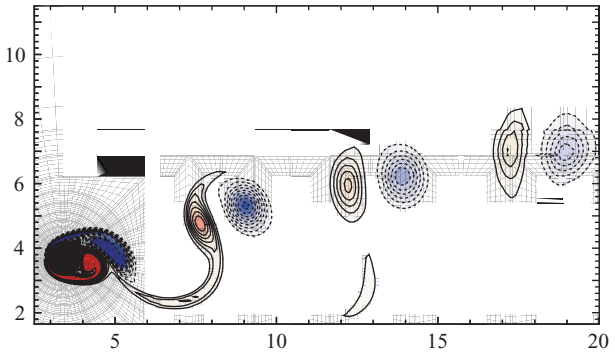

FIGURE 7. Vorticity field ω_z for $m^* = 0.1$, $L^* = 5.0$ and $Fr = 0.8$, for the cylinder at the top of the oscillation cycle. Contours are evenly spaced over the range (blue) $-5.0 \leqslant \omega_z \leqslant 5.0$ (red); with $\Delta\omega_z = 0.5$.

in the positive y-direction. At this position in the oscillation cycle, both a negative and a positive vortex structure are forming behind the cylinder. The instantaneous streamlines indicate that the motion of the cylinder is inducing an upstream and positive y-component of velocity in the fluid directly behind the cylinder. This acts to move the positive vortex core upstream and in the positive y-direction, and increases the intensity of the negative vortex core.

Figure 8(b) shows the instantaneous vortex structures a quarter of a cycle later. Here, the cylinder is at the top of its cycle (i.e. the most anticlockwise position) and is stationary. The negative vortex core has commenced convecting downstream. The motion of the cylinder prior to this snapshot has drawn the positive vortex core upstream and in the positive y-direction, such that it is now directly behind the cylinder. Importantly, when compared to the case of a stationary cylinder, the positive vortex is closer to the newly shed negative vortex core. The negative vortex core is stretched around the positive vortex core, and from the instantaneous streamlines, a jet of fluid has formed between the two vortex cores. The jet is travelling both in the upstream and positive y-direction.

In figure 8(c), the cylinder is midway between the top and bottom of the oscillation cycle, and is moving in a downstream and negative y-direction. The positive vortex core has shed from the cylinder, and is positioned downstream and above the rear cylinder surface. While the positive vortex core has shed, it remains close to the cylinder surface. As may be seen from the instantaneous streamlines, the position of the positive vortex core inhibits the growth of the developing negative vortex core, which is located at the cylinder surface. The jet between the shed positive and negative vortices is now directed principally in the positive y-direction. In this snapshot, the shed negative vortex core is still considerably elongated in the cross-stream direction.

In figure 8(d), the cylinder is at the bottom of its oscillation cycle and is instantaneously stationary. The positive vortex core has convected further downstream allowing the developing negative vortex core to grow slightly. However, from the instantaneous streamlines, the growth of the developing negative core is still inhibited by the position of the positive vortex core. At this point, the shed positive vortex core has been stretched in the cross-stream direction and is becoming more diffuse. By contrast, the shed negative vortex core maintains its intensity over a small area, and is becoming less elongated. It appears that the jet acting in the positive y-direction,

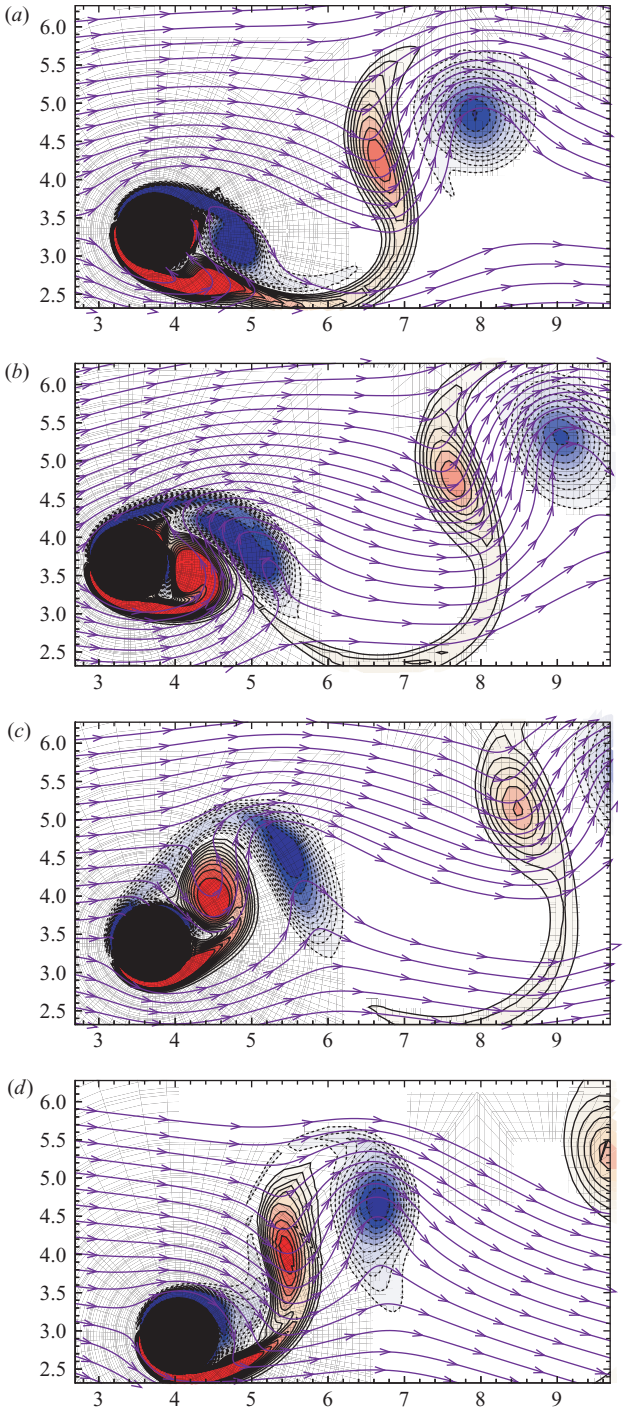

FIGURE 8. Vorticity field ω_z for $m^* = 0.1$, $L^* = 5.0$ and $Fr = 0.8$: (*a*) for the cylinder moving from the bottom of the oscillation cycle to the top of the oscillation cycle; (*b*) for the cylinder at the top of the oscillation cycle; (*c*) for the cylinder moving between the top of the oscillation cycle and the bottom of the oscillation cycle; (*d*) for the cylinder at the bottom of the oscillation cycle. Contours are evenly spaced over the range (blue) $-5.0 \leqslant \omega_z \leqslant 5.0$ (red); with $\Delta\omega_z = 0.5$.

combined with the free-stream velocity maintains the intensity of the negative vortex core.

Returning briefly to figure 8(*a*), it may be seen that the combined action of the jet and the free-stream velocity continue to maintain a small intense negative vortex core as the vortex pair convect downstream.

In summary, the motion of the cylinder as it moves from the bottom to the top of the oscillation cycle acts to induce the positive vortex core to move upstream and in the positive y-direction. The subsequent position of the positive vortex core induces a jet between itself and the newly shed negative vortex core. The position of the positive vortex core also inhibits the growth of the developing negative vortex core. This results in a delay of the shedding of the negative vortex cores and allows vortex pairing in the wake. A jet forms between each shed vortex pair, which induces a momentum shift from the inflow direction to the crossflow direction, inducing a negative mean lift. A momentum balance of the narrow intense jet (directed upward) and the broader less-intense jet (directed downward) supports this supposition. From this analysis, the following hypothesis may be formed:

> 'The negative mean lift is due to the inclined angle to the free stream at which the cylinder oscillates.'

As discussed in the Introduction, very few studies have analysed the motion of a cylinder confined to oscillate at an angle other than 90° or 0° to the flow field. Of these, only the numerical work of Kocabiyik (2003) has identified a finite mean lift force. Kocabiyik (2003) restricted the motion of the cylinder such that upstream oscillations coincided with a negative y-oscillation and downstream oscillations coincided with a positive y-oscillation (i.e. the angle of oscillation of the cylinder was essentially 90° from that described in the present study). She found a positive mean lift occurred for a wide range of oscillation amplitudes.

3.2. *The effect of varying the tether length*

In this section, we investigate the effect of varying the normalized tether length parameter ($L^* = L/D$). For a majority of the results reported in this section, the parameter space has been restricted to consider only $m^* = 0.2$; however, in § 3.2.5 this restriction is removed and we determine the critical mass ratio, m^*_{crit} (as defined in § 3.1.5 for a tethered cylinder) as a function of tether length.

The value of $m^* = 0.2$ was chosen, because, for the case of $L^* = 5$, the large-amplitude oscillation branch was noted for $Fr \geqslant 0.8$ for this mass ratio. This branch of tethered cylinder response exhibits large oscillation amplitudes of up to $0.5D$, and it is therefore interesting to examine if this mode exists for both larger and smaller tether lengths.

Tether length ratios in the range $L^* = [1, 10]$ were investigated. As the tether length is measured from the centre of the cylinder, $L^* < 0.5$ would represent a cylinder which is pivoted internally. The limiting case of L^* for very small tethers is $L^* \to 0$, where $L^* = 0$ represents a cylinder which may undergo pure rotational oscillations about its centre.

As the tether length increases, the amount of curvature for a given oscillation amplitude decreases. For example, for $L^* = 15$, and $A^* = 0.5$, the angular amplitude, θ' is only 1.9°. This may be compared with the same amplitude, A^*, for tether length, $L^* = 5$ ($\theta' \simeq 5°$) and for a tether length $L^* = 1$ ($\theta' \simeq 26.6°$).

For large tether lengths the tethered cylinder closely approximates a freely oscillating cylinder restricted to oscillate at an angle to the flow field, where the angle of oscillation is defined by (3.1). For large tether lengths, the curvature of the cylinder

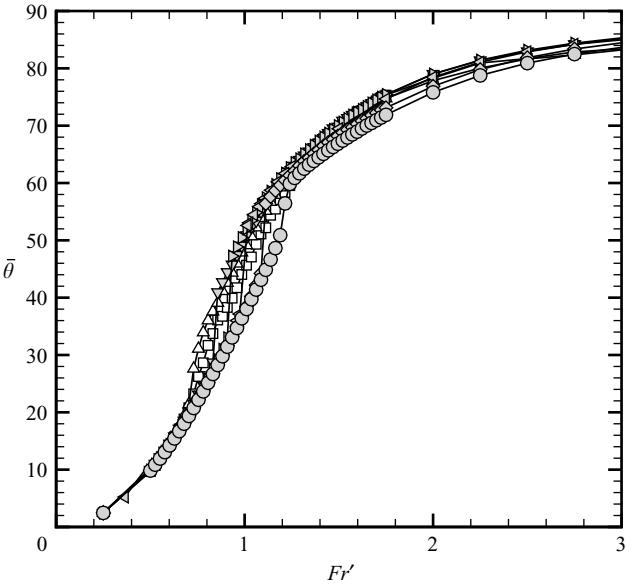

FIGURE 9. Mean layover angle as a function of reduced Froude number for $m^* = 0.2$ and $L^* \in [1, 10]$. □, $L^* = 1.0$. △, $L^* = 2.0$; ∇, $L^* = 3.0$; ▷, $L^* = 4.0$; ◁, $L^* = 5.0$; ◆, $L^* = 7.5$; ●, $L^* = 10.0$.

path, represented by the angular amplitude, θ', varies with the amplitude of oscillation in the direction of motion, A^*, as

$$\theta' = \tan^{-1}\left(\frac{A^*}{L^*}\right). \tag{3.2}$$

The study of large tether lengths provides a link between research on a tethered cylinder and prior studies on freely oscillating cylinders with low mass and damping (see for example Khalak & Williamson 1999 and Govardhan & Williamson 2000). Of particular interest is the effect of the tether length on the critical mass ratio, m^*_{crit}, when compared with that found for a freely oscillating cylinder at the same Reynolds number (see Ryan *et al.* 2004*b*), and whether the imposed oscillation angle has any significant effect on the cylinder response.

3.2.1. *Mean layover angle results*

Figure 9 shows the mean layover angle as a function of reduced Froude number for $L^* = [1, 10]$. An excellent collapse of data is observed. The results show an inflection at $\overline{\theta} \simeq 45^\circ$ at $Fr' \simeq 1$. Below $Fr' \simeq 1$ the rate of change of $\overline{\theta}$ is considerably greater than for $Fr' > 1$. If we consider (3.1) (rewritten below), relating the mean layover angle to the mean hydrodynamic force components, this collapse of data is perhaps not too surprising:

$$\overline{\theta} = \tan^{-1}\left(\frac{\overline{C_D}}{\overline{C_L} + \pi/2Fr'^2}\right) \tag{3.3}$$

The right-hand side of (3.3) is virtually independent of tether length, although it is anticipated that there is some variation in $\overline{C_D}$ and $\overline{C_L}$ with tether length. Therefore, (3.3) implies that the mean layover angle must also be virtually independent of tether length.

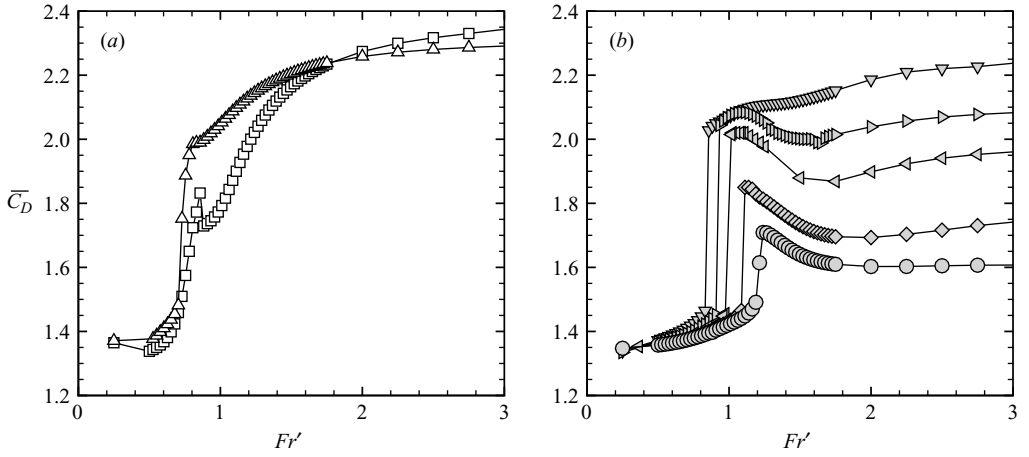

FIGURE 10. Mean drag coefficient as a function of reduced Froude number for $m^* = 0.2$ and $L^* \in [1, 10]$. (*a*) $L^* = 1.0$ and 2.0, (*b*) $L^* \in [3.0, 10.0]$. Symbol definitions are the same as for figure 9.

While not apparent from the results in this figure, all tether length cases exhibit a jump in the mean layover angle for this mass ratio ($m^* = 0.2$). However, for the case of $L^* = 1.0$, this discontinuous increase is comparatively small. Interestingly, the reduced Froude number where the jump is observed increases proportionately with tether length.

3.2.2. *Mean drag coefficient results*

Figure 10 shows the mean drag coefficient as a function of reduced Froude number for $L^* = [1, 10]$ and $m^* = 0.2$. On the left-hand side are tether lengths $L^* = 1.0$ and 2.0; on the right-hand side are tether lengths $L^* \in [3.0, 10.0]$. For a majority of tether lengths investigated, a jump in $\overline{\theta}$ was observed as the reduced Froude number was increased beyond a critical value.

Considering figure 10, as the reduced Froude number is increased, the drag coefficient is observed to undergo a discontinuous increase for all tether lengths considered. For tether lengths in the range $L^* \in [2.0, 10.0]$, a discontinuous jump is observed at a critical Froude number. The value of the critical Froude number is observed to increase slightly with tether length. Further, the maximum drag coefficient observed decreases with increasing tether length. For $L^* = 1.0$, the response of the mean drag coefficient is found to be markedly different. While a small jump in $\overline{C_D}$ is observed, it is markedly reduced when compared with larger tether lengths. Further, a small, discontinuous decrease in $\overline{C_D}$ is observed at $Fr' \simeq 0.9$. Following this discontinuity, $\overline{C_D}$ increases smoothly with increasing Fr'.

Considering the mean drag results for all the tether lengths considered in figure 10, it is observed that a significant variation in the maximum value of the mean drag coefficient exists as a function of tether length. As the mean drag was shown to vary with oscillation amplitude in § 3.1.4, it is interesting to determine the maximum mean drag as a function of tether length, as this may reflect the maximum amplitude of oscillation expected.

We determined the maximum mean drag coefficient for a wide range of tether lengths ($L^* = [0.8, 10]$); the results of this study are shown in figure 11. For the range $L^* = [2, 10]$, the maximum mean drag is observed to decrease with L^*. We may

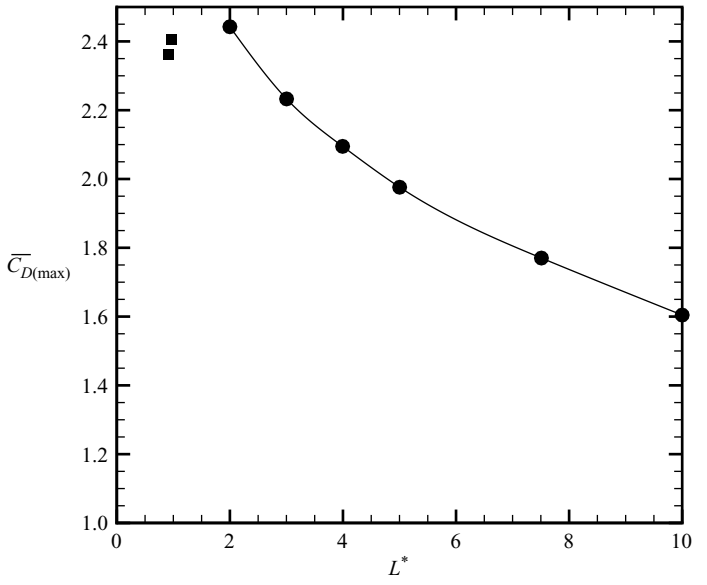

FIGURE 11. Maximum value of mean drag coefficient across all reduced Froude numbers considered, as a function of normalized tether length for $m^* = 0.2$. ■, $L^* \leqslant 1.0$, ● $L^* > 1.0$; for $L^* \leqslant 1.0$, the maximum mean drag coefficient was found to grow with increasing tether length. For higher tether lengths, the maximum mean drag was found to decrease with increasing tether length.

approximate this decrease with the equation

$$\overline{C_{D(\max)}} = 1.6071\mathrm{e}^{-0.127L^*} + 1.15. \tag{3.4}$$

In this equation, the constant 1.15 is the mean drag coefficient calculated for a freely oscillating cylinder with $m^* = 0.2$ at $Re = 200$, for an infinite reduced velocity and no damping (see Ryan *et al.* 2004*b*). Equation (3.4) reveals that the maximum mean drag coefficient decreases with tether length, such that, for the case of $L^* \to \infty$, the mean drag response approaches the case of a freely oscillating cylinder with no damping and $u^* = \infty$. For tether lengths $L^* < 2$ the maximum mean drag coefficient begins to decrease. Assuming that the variation in the maximum mean drag coefficient is due to the oscillation of the cylinder, it should be expected that as $L^* \to 0$ the mean drag approaches that observed for a fixed cylinder ($\overline{C_D} \simeq 1.36$ for a fixed cylinder with $Re = 200$).

3.2.3. *Mean lift coefficient*

Figure 12 shows the mean lift coefficient as a function of Fr' for $L^* = [1, 10]$ and $m^* = 0.2$. As was previously shown in § 3.1.3, for $L^* = 5$ a negative mean lift coefficient is noted for a majority of reduced Froude numbers investigated. As expected, this overall trend is noted for the entire range of tether lengths considered here.

For all tether lengths investigated, there was a value of Fr' at which a local minimum in $\overline{C_L}$ was observed. The value of Fr' at which this local minimum is observed varies slightly with tether length; however, it is always found in the range $Fr' = [0.8, 1]$. Interestingly, a very small *positive* mean lift coefficient was found for the case of $L^* = 1$ and 2 for $Fr' \gtrsim 2$. This implies that for these two cases there is a difference in the shedding process in this range of Fr' when compared to longer tether length cases with the same inflow conditions. While not shown in figure 12, this positive lift

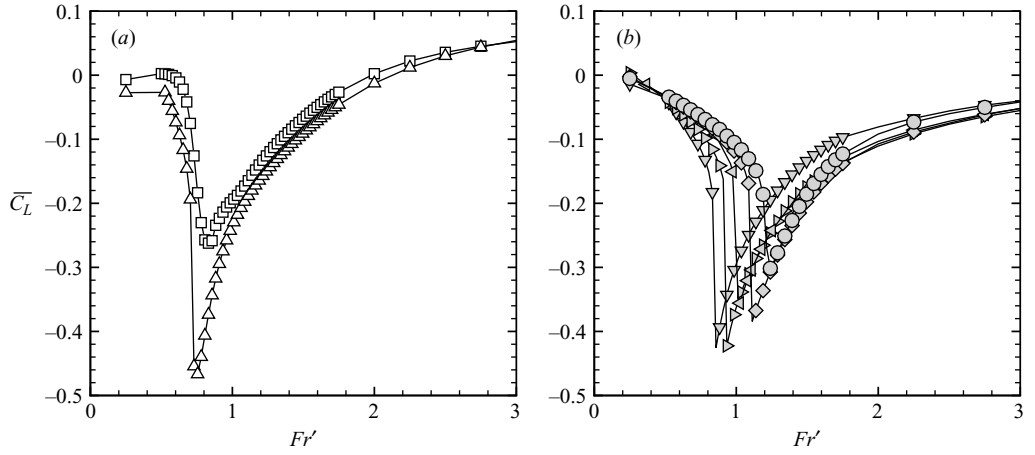

FIGURE 12. Mean lift coefficient as a function of the reduced Froude number, Fr', for $m^* = 0.2$ and $L^* = [1, 10]$. (*a*) $L^* = 1.0$ and 2.0, (*b*) $L^* \in [3.0, 10.0]$. Symbol definitions are the same as for figure 9.

coefficient was observed up to $Fr' \simeq 10.0$. Ryan (2004) reported that the recording of a positive mean lift occurs in conjunction with a highly asymmetrical wake, for both cases of $L^* = 1.0$ and 2.0, as $\overline{\theta} \to 90°$. From observation, this small positive mean lift is due to a minor asymmetry of the wake for these tether lengths and mean layover angles. For higher values of Fr', corresponding to $\overline{\theta} \to 90°$, the mean lift approaches zero for all tether lengths considered.

In § 3.1.6, it was hypothesized that the negative mean lift coefficient could be due to a combination of the oscillation amplitude, and the angle between the flow direction and the cylinder motion. An alternative hypothesis is that it could be due to the imposed curvature on the motion of the cylinder by the tether. The observation that the local minimum in $\overline{C_L}$ occurs at $\overline{\theta} \simeq 50°$, regardless of tether length in the range $L^* = [2.0, 5.0]$, lends weight to the first hypothesis. The small variation in the minimum value of $\overline{C_L}$, as a function of L^* in the range $L^* = [2.0, 5.0]$, indicates a correspondingly small variation in the amplitude of oscillation in this range of L^*. This variation in amplitude is discussed in the next section.

3.2.4. *Amplitude of oscillation results*

Figure 13 shows the amplitude of oscillation, A^*, as a function of the reduced Froude number, Fr', for tether lengths in the range $L^* = [1.0, 10.0]$ and $m^* = 0.2$. For all tether lengths investigated, a rapid increase in A^* was noted as Fr' was increased beyond $Fr' \simeq 1$. The dramatic increase in A^* as a function of Fr' corresponds to the rapid increase noted for $L^* = 5$ and $m^* < m^*_{crit}$ described in § 3.1.4 and § 3.1.5.

In § 3.1.5, for $m^* \leqslant m^*_{crit}$ and $L^* = 5.0$, the increase in A^* as a function of Fr' was described as discontinuous. From figure 13, the increase in A^*, as a function of Fr', is clearly discontinuous for $L^* = [3.0, 7.5]$. However, for $L^* = 1.0$ and 2.0, the amplitude increases rapidly but smoothly as a function of Fr'. For $L^* = 10.0$, there is a discontinuous jump at $Fr' \simeq 1.1$; however, this jump is considerably smaller when compared to other tether length results. As will be shown in § 3.2.5, for $L^* = 10.0$, m^*_{crit} is very close to and possibly marginally smaller than for the case of $m^* = 0.2$ shown here. Should m^*_{crit} be less than 0.2 for $L^* = 10.0$, then the amplitude should increase

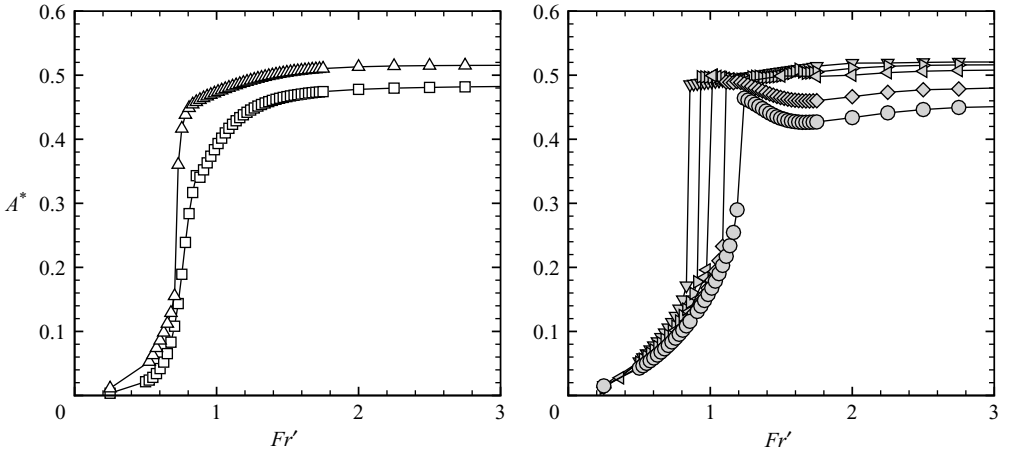

FIGURE 13. Amplitude of oscillation, in the direction of motion, as a function of the reduced Froude number, Fr', for $m^* = 0.2$ and $L^* = [1, 10]$. (*a*) $L^* = 1.0$ and 2.0, (*b*) $L^* \in [3.0, 10.0]$. Symbol definitions are the same as for figure 9.

smoothly, in a fashion similar to the case of $m^* = 0.4$ and $L^* = 5.0$ shown previously in § 3.1.4.

For $Fr' > [0.8, 1.0]$, the amplitude of oscillation quickly reaches a steady value invariant of further increases in Fr', up to and including the highest Fr' investigated (here $Fr'_{\max} = 50$). This amplitude corresponds to the highest amplitude observed for the range of Fr' investigated. Of interest is that this maximum value of A^* varies only slightly with tether length. A high maximum amplitude is observed even at small tether lengths as low as $L^* = 1.0$.

Figure 14 shows the maximum amplitude of oscillation as a function of L^* across all Fr' considered in this investigation. For $L^* \geqslant 3.0$, the amplitude decreases slowly with increasing tether length. The maximum amplitude observed across all tether lengths investigated occurs at $L^* \simeq 3.0$. Comparing figure 11 with figure 14, a similarity in the response of $\overline{C_{D(\max)}}$ as a function of L^*, and $A^*_{\max}$ as a function of L^*, is observed. This supports the hypothesis that the mean drag coefficient may be related directly to the amplitude of oscillation, as discussed previously in § 3.2.2.

3.2.5. *The critical mass ratio as a function of tether length*

The final part of the results section considers the variation of the critical mass ratio with tether length. It was noted in § 3.1.2 that the critical mass ratio at which a discontinuous jump in A^*, $\overline{C_D}$ and $\overline{\theta}$ was observed was approximately $m^* = 0.36$. This value is considerably higher than that found for the hydro-elastically mounted cylinder at the same Reynolds number (see Ryan *et al.* 2004*b*), and it is therefore reasonable to assume that m^*_{crit} varies as a function of L^*. Further supporting evidence may be found when considering the equation of motion as $L^* \to \infty$. In this case, the equation of motion reverts to the same form as that found by Govardhan & Williamson (2003) for the case of a hydro-elastically mounted cylinder; albeit that the current equation allows the cylinder to oscillate at a mean layover angle to the flow, where the angle is specified by the mean hydrodynamic forces acting on the cylinder.

This raises the question of why should a hydrodynamically mounted cylinder oscillating at a mean layover angle (other than transverse) to the free stream have the

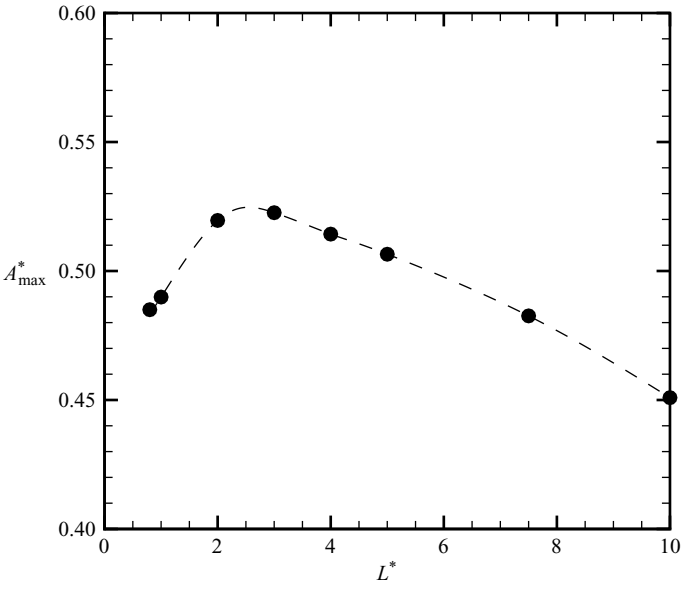

FIGURE 14. Maximum amplitude of oscillation, in the direction of motion, as a function of L^*, for $m^* = 0.2$.

same m^*_{crit} when compared to previous studies, which have only considered cylinders mounted such that they are restricted to move transverse to the free stream?

Based on the results already presented in this paper, a partial answer to this question can be made. Referring back to figure 9, we see that the jump in $\overline{\theta}$ occurs at roughly the same $\overline{\theta}$ in each case, regardless of tether length. For the special case of a buoyant tethered cylinder, this corresponds to the jump in $\overline{\theta}$ occurring at approximately the same reduced Froude number. This is simply due to the fact that the reduced Froude number controls the mean hydrodynamic forces acting on the cylinder, and hence controls the mean layover angle. From this perspective, for $m^* < m^*_{crit}$ it is reasonable to expect the jump to occur at roughly the same Fr' irrespective of tether length (as observed in this study).

Considering the amplitude results for $m^* < m^*_{crit}$ in all the cases reported thus far, we observe that once the critical Fr' is exceeded, the amplitude of oscillation remains relatively constant up to the largest Fr' considered (corresponding to $\overline{\theta} \to 90^0$). Therefore, from our findings, we may conservatively predict that when comparing several mass ratios at a given tether length and at $\overline{\theta} \to 90^0$, any jump in A^* as a function of m^* would also be observed for any layover angle beyond the critical value of Fr'. This result is clear when considering either figure 5 or 13.

In this section we consider the variation in system response as we vary m^* for various tether lengths; however, given the previous discussion we will restrict our attention to the case where $\overline{\theta} \to 90^0$, i.e. the fully laid over case. This reduces the mean lift to zero, and therefore most closely approximates the case of a hydro-elastically mounted cylinder mounted to oscillate transverse to the free stream. The previous results also provide sufficient evidence to believe that the critical mass ratio observed as $\overline{\theta} \to 90^0$ is the same as that observed at lower $\overline{\theta}$ values. To obtain these large layover angles, the reduced Froude number was fixed for all the following simulations such that $Fr' = 50$.

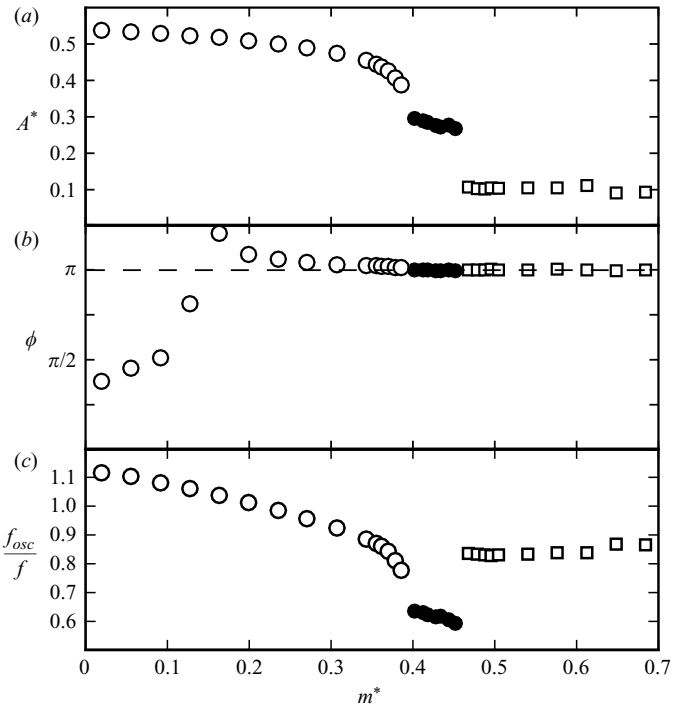

FIGURE 15. (*a*) Amplitude of oscillation, (*b*) phase lag between the oscillation and forcing signal, and (*c*) frequency ratio of a tethered cylinder oscillating at $Fr' = 50$; for $m^* = [0.02, 0.72]$ and $L^* = 5$.

We commence by once again considering the case of $L^* = 5.0$. Figure 15 shows the response of the system over the range of mass ratios $m^* = [0.02, 0.7]$. Three response modes are observed, which we will tentatively refer to as the 'upper', 'lower', and 'small-amplitude' modes of oscillation. These modes have been named as there are several similarities in the response when compared to the low mass-damped hydro-elastically mounted cylinder.

Figure 15(*a*) shows the oscillation amplitude as a function of m^*. We observe that for $m^* < m^*_{crit}$ (hollow circles) a large-amplitude oscillation is observed. This amplitude decays gradually with increasing mass ratio. As $m^* \rightarrow m^*_{crit}$, the rate of decay in A^* increases significantly until at $m^* = m^*_{crit}$, a discontinuous decrease in A^* is observed as the system changes from the 'upper' mode to the 'lower' mode of oscillation. In the range $m^* = [0.38, 0.46]$, corresponding to the 'lower' mode of shedding (filled circles), the amplitude remains reasonably high. However, the data clearly show a linear decline in amplitude with increasing m^*. A dramatic reduction in A^* is observed at $m^* \simeq 0.47$ as the system changes from the 'lower' branch to the 'small-amplitude' branch of oscillation. For mass ratios beyond this second discontinuous decrease in A^*, only very small amplitudes are observed. Within this mode, the amplitude of oscillation is remarkably constant irrespective of any further increases in m^*.

Figure 15(*b*) considers the phase lag between the oscillation force in the direction of motion, defined by equation (1.6), and the cylinder oscillation itself. It is this force component which drives the oscillations observed and includes both the vortex and potential force components. Following the work of Khalak & Williamson (1999), we obtain the phase lag between these two signals by taking the Hilbert transform of

both signals, which provides the instantaneous phase for each signal. By then taking the averaged difference between these phase lags for each signal, we were able to obtain the average phase lag between the forcing and oscillation signals.

We observe that the only variation in the phase lag occurs within the upper mode. When considering the results of Govardhan & Williamson (2003) for the case of the hydro-elastically mounted cylinder, a change in the total phase is noted at the transition from the upper to the lower branch of oscillation. More recent studies of the hydro-elastically mounted cylinder, at significantly lower Reynolds numbers (comparable to the current study), by Leontini *et al.* (2006) indicate that a steady variation of the total phase may be observed within a branch of shedding which is qualitatively similar to the results in figure 15(*b*). For m^* in the range 0.16 to 0.38, the results indicate that the phase is greater than 180^0; that is, the motion leads the input force. Assuming that both the force signal and the oscillation signal are simple sinusoids with the same fundamental frequency, this would indicate that energy is being transferred from the cylinder to the fluid. An energy transfer such as this is unsustainable over a single period of oscillation.

This somewhat odd result is clarified if we consider the time histories of both the force and the oscillation of the cylinder (see figure 16). Each panel shows the oscillation signal (solid line) and the oscillation force signal (dashed line) over 4 cycles of oscillation. Figure 16(*a*) shows the results for $m^* = 0.02$. Here, both the oscillation trace and the force trace clearly show the same dominant frequency and are in phase. Increasing the mass ratio to $m^* = 0.16$ (figure 16*b*), which shows the largest phase lag in figure 15, we observe a significant change. Here the forcing signal has two dominant frequency components; however, the oscillation still shows a profile similar to the lower mass ratio case, and is clearly dominated by one frequency component. This variation in the frequencies dominating the force and the oscillation signals accounts for the discrepancy observed with the phase lag. In this study, the phase lag is defined as the lag of the motion signal behind the force signal. Here, the frequency of the motion trace is used when determining the frequency at which the phase lag should be calculated. As the force trace has more than one frequency for $m^* = 0.16$, it is possible that the phase lag may be greater than 180^0. This indicates that the energy to drive the motion is derived from higher-frequency force components.

As the mass ratio is increased further, the forcing signal gradually becomes more dominated by a single frequency, until, once the system is oscillating in the 'lower' mode, the same frequency is observed for both the oscillation and the forcing signals, and the two signals are clearly out of phase (figure 16*c*).

Referring back to figure 15(*c*), we observe that there is a significant variation in the frequency of oscillation when the system changes from one mode to another. In this figure, the frequency of oscillation has been normalized by the shedding frequency of a fixed cylinder. It is clear for both the 'upper' and the 'lower' modes of oscillation that the frequency of oscillation drives the shedding frequency, and therefore the shedding is said to be 'synchronized' with the oscillation frequency. Given the time traces in figure 16, the fact that f_{osc}/f passes through unity in the 'upper' branch probably explains why two frequency components are observed in the forcing signal. For example, for $m^* = 0.16$, $f_{osc}/f \simeq 1$, which may induce a beating effect with the natural shedding frequency from a fixed cylinder. This beating effect is lessened as the mass ratio is increased and the oscillation frequency moves away from the shedding frequency of a fixed cylinder.

A significant transition in the oscillation frequency is observed as the cylinder oscillations move from the 'upper' to the 'lower' mode. In the 'lower' mode, the

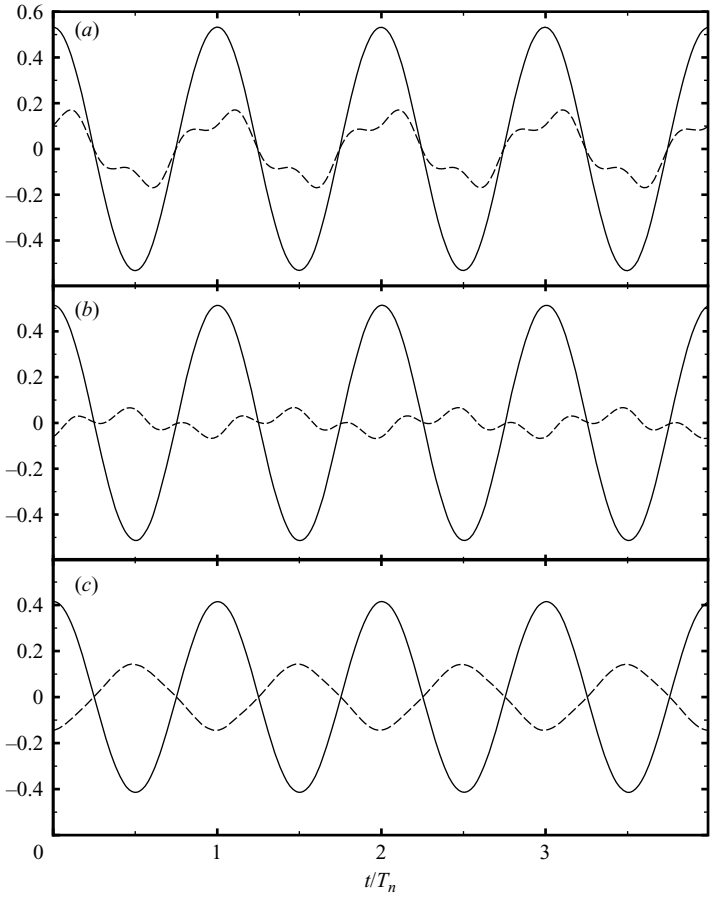

FIGURE 16. Time trace of (solid line) oscillation, and (dashed line) fluid forcing acting on the tethered cylinder. (*a*) $m^* = 0.02$, (*b*) $m^* = 0.16$, and (*c*) $m^* = 0.38$. In each case $L^* = 5$ and $Fr' = 50$.

cylinder oscillations are clearly driving the shedding, and the results are reminiscent of the 'lower' branch for the hydro-elastically mounted cylinder described by Govardhan & Williamson (2003). Also of note is the 'low-amplitude' mode; here the frequency of oscillation approaches the shedding frequency for a fixed cylinder, but up to the highest m^* considered, the value of f_{osc}/f never reaches unity.

Having carefully described the modes observed for $L^* = 5.0$, we are now in a position to consider the effect of varying the tether length on the cylinder motion. In particular, we wish to determine the critical mass ratio as a function of tether length, that is, the mass ratio at which we observe a transition from the 'upper' to the 'lower' modes of oscillation.

Figure 17 shows the amplitude of oscillation results for a range of mass ratios for tether lengths $L^* = 5.0, 10, 20$ and 50. For each case, the transition from the 'upper' mode to the 'lower' mode is clearly evident. Two points are clear from this figure. The first is that the critical mass ratio at which a transition from the 'upper' to the 'lower' mode of oscillation decreases with increasing tether length. Second, the average amplitude of oscillation in the 'lower' mode of oscillation is observed to increase slightly with decreasing tether length. It is apparent that for the limiting case

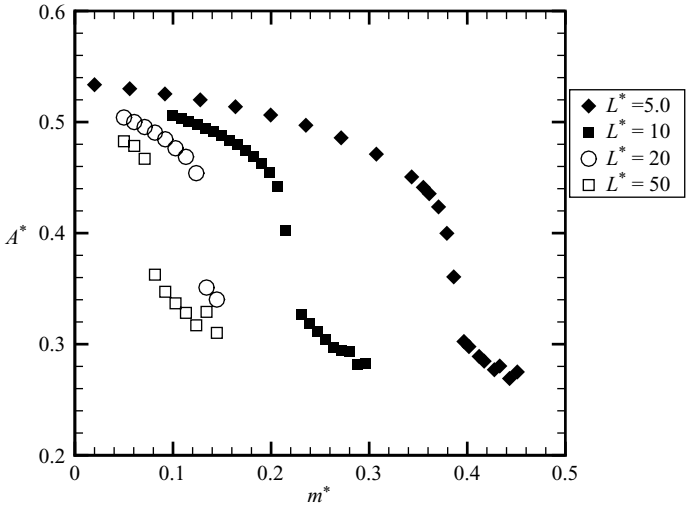

FIGURE 17. Amplitude of oscillation as a function of mass ratio for various tether length ratios; in each case $Fr' = 50$.

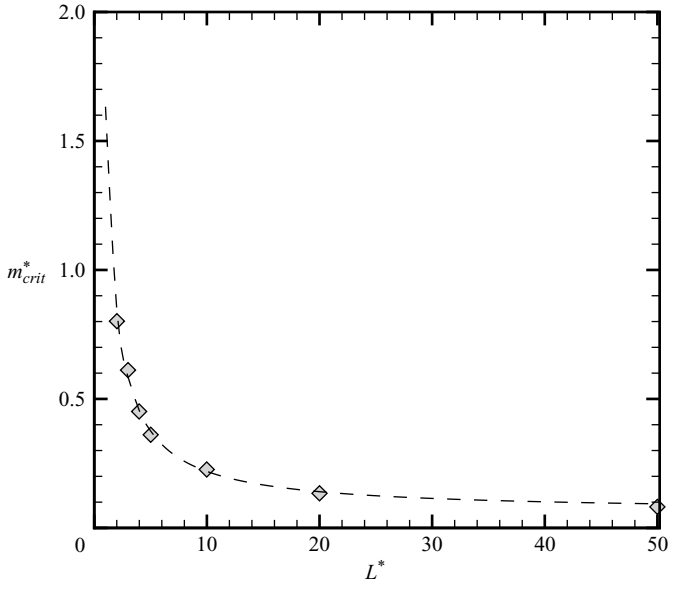

FIGURE 18. Mean layover angle as a function of reduced velocity for $m^* = 0.2$ and $L^* = [1, 10]$.

of $m^* \to 0$, an amplitude of oscillation of $A^* \simeq 0.5$ is observed independent of tether length.

The same study has been performed over a range of tether lengths ($L^* = [2, 50]$) and the findings are shown in figure 18. Here the variation in critical mass ratio as a function of tether length is apparent. A fit of the data has been made, and it was found for $Re = 200$ that

$$m^*_{crit} = 0.062 + \frac{\pi}{2L^*}. \tag{3.5}$$

This fit implies that as $L^* \to \infty$, the critical mass ratio will approach 0.062 for $Re = 200$. It is assumed that this value should approximate the critical mass ratio for the case of a freely oscillating cylinder with no restoring force at $Re = 200$. Prior work by Ryan, Thompson & Hourigan (2004*b*) has been performed on the hydro-elastically mounted cylinder at low Reynolds numbers and has indicated that for $Re = 190$ to 200 the critical mass ratio is approximately $m^*_{crit} = 0.6$ to 0.95. This agrees remarkably well with the present findings, especially when it is considered that the critical mass ratio was found to vary significantly over this Reynolds number range ($Re = [190, 200]$) for the hydro-elastically mounted cylinder study. The agreement is more remarkable when considering the uncertainty in the extrapolation (equation (3.5)) for infinitely long tether lengths.

4. Conclusion

Several important results on the motion of a tethered cylinder in a uniform flow have been presented in this paper. In this section, we wish to direct the reader's attention to some of the implications of these findings with respect to the original aims raised within the Introduction.

First, we can make some general comments regarding the effect of varying both mass ratio and tether length ratio on the response of the tethered cylinder system. For low Froude numbers, the results collapse onto a line regardless of mass ratio. Beyond a critical range of reduced Froude number ($Fr'_{crit} > [0.8, 1.0]$), a jump is observed for systems with sufficiently low mass ratio. The remainder of this discussion considers $Fr' > Fr'_{crit}$.

In general, increasing the mass ratio of the system reduces the amplitude of oscillation. This reduction is not smooth. There is a critical mass ratio at which a discontinuous decrease in the amplitude of oscillation is observed, and for slightly higher mass ratios beyond m^*_{crit}, a further discontinuous decrease in amplitude is observed. For $m^* > m^*_{crit}$ the amplitude of oscillation collapses fairly well independent of reduced Froude number, and at high Froude numbers, the amplitude of oscillation decays to small values. For sufficiently small mass ratios, $m^* < m^*_{crit}$, the increase in amplitude observed at $Fr' \simeq Fr'_{crit}$ is accompanied by an increase in mean hydrodynamic force coefficients. Hence, for sufficiently small mass ratios, a discontinuous jump in the mean layover angle is associated with the increase in oscillation amplitude. Varying the tether length has little effect on the response of the system provided that $m^* < m^*_{crit}$ for all tether lengths considered. However, m^*_{crit} is observed to monotonically decrease with increasing tether length.

It is postulated that the definition of m^*_{crit} developed here is analogous to that of a hydro-elastically mounted cylinder. The critical mass ratio varies as a function of tether length. This is due to nonlinear terms in the equation of motion for finite tether lengths. For large tether lengths, the nonlinear terms are very small and the critical mass ratio for the tethered cylinder approaches the value observed for a hydro-elastically mounted cylinder at the same Reynolds number.

Oscillation of the cylinder system induces a negative mean lift due to a vortex pairing structure in the cylinder wake. For similar mean layover angles, this structure is observed independent of tether length.

The first author would like to acknowledge support provided through a Monash Departmental Scholarship. The authors would like to acknowledge strong support from an Australian Research Council Discovery Grant, the Victorian Partnership

for Advanced Computing and the Australian Partnership for Advanced Computing, which enabled this research to take place.

REFERENCES

Bearman, P. W. 1984 Vortex shedding from oscillating bluff bodies. *Annu. Rev. Fluid Mech.* **16**, 195–222.

Blackburn, H. M. & Henderson, R. D. 1999 A study of two-dimensional flow past an oscillating cylinder. *J. Fluid Mech.* **385**, 255–286.

Blevins, B. 1990 *Flow-Induced Vibrations*. Van Nostrand Reinhold.

Browne, P., Carberry, J., Hourigan, K. & Sheridan, J. 2005 Study of a tethered cylinder in a free stream. In *Proc. Intl. Conf. on Bluff Body Wakes and Vortex Induced Vibrations 4* (BBVIV4), pp. 29–32.

Carberry, J. J. & Sheridan, J. 2007 Wake states of a tethered cylinder. *J. Fluid Mech.* (to appear).

Govardhan, R. N. & Williamson, C. H. K. 2000 Modes of vortex formation and frequency response of a freely vibrating cylinder. *J. Fluid Mech.* **420**, 85–130.

Govardhan, R. N. & Williamson, C. H. K. 2003 Resonance forever: Existence of a critical mass and an infinite regime of resonance in vortex-induced vibration. *J. Fluid Mech.* **473**, 147–166.

Griffin, O. M. & Ramberg, S. E. 1982 Some recent studies of vortex shedding with application to marine tubulars and risers. *ASME J. Energy Resour. Technol.* **104**, 2–13.

Hourigan, K., Thompson, M. C. & Tan, B. T. 2001 Self-sustained oscillations in flows around long blunt plates. *J. Fluids Struct.* **15**, 387–398.

Khalak, A. & Williamson, C. 1999 Motions, forces and mode transitions in vortex-induced vibrations at low mass-damping. *J. Fluids Struct.* **13**, 813–851.

Kocabiyik, S. & Al-Mdallal, Q. 2003 A numerical study on the recti-linear oscillations of a circular cylinder in cross-flow: Flow patterns and loading. In *Proc. IUTAM Symp. on Integrated Modeling of Fully–Coupled Fluid Structure Interactions Using Analysis, Computations and Experiments*, pp. 163–173. Kluwer.

Lamb, H. 1932 *Hydrodynamics*. Dover.

Leontini, J. S., Thompson, M. C. & Hourigan, K. 2006 The beginning of branching behaviour during vortex-induced vibration at 2-D Reynolds numbers. *J. Fluids Struct.* **22**, 857–864.

Naudascher, E. & Rockwell, D. 1994 *Flow-Induced Vibrations: An Engineering Guide*. Balkema.

Newman, J. 1977 *Marine Hydrodynamics*, 1st edn. MIT Press.

Parkinson, G. 1989 Phenomena and modelling of flow-induced vibrations of bluff bodies. *Prog. Aerospace Sci.* **26**, 169–224.

Pregnalato, C. J. 2003 Flow-induced vibrations of a tethered sphere. PhD thesis, Department of Mechanical Engineering, Monash University.

Ryan, K. 2004 The analysis of wake structures behind stationary, freely oscillating and tethered cylinders. PhD thesis, Department of Mechanical Engineering, Monash University.

Ryan, K., Pregnalato, C., Thompson, M. & Hourigan, K. 2004*a* Flow-induced vibrations of a tethered circular cylinder. *J. Fluids Struct.* **19**, 1085–1102.

Ryan, K., Thompson, M. C. & Hourigan, K. 2004*b* Vortex structures in the wake of a buoyant tethered cylinder at moderate to high reduced velocities. *Euro. J. Fluid Mech.* B **23**, 127–135.

Ryan, K., Thompson, M. C. & Hourigan, K. 2005 Variation in the critical mass ratio of a freely oscillating cylinder as a function of Reynolds number. *Phys Fluids* **17**, 038106.

Sarpkaya, T. 1979 Vortex-induced oscillations. *J. Appl. Mech.* **46**, 241–258.

Sheard, G., Thompson, M. & Hourigan, K. 2003 From spheres to circular cylinders: Stability and flow structures of bluff ring wakes. *J. Fluid Mech.* **492**, 147–180.

Shiels, D., Leonard, A. & Roshko, A. 2001 Flow-induced vibration of a circular cylinder at limiting structural parameters. *J. Fluids Struct.* **15**, 3–21.

Thompson, M. C., Hourigan, K. & Sheridan, J. 1996 Three-dimensional instabilities in the wake of a circular cylinder. *Exp. Therm. Fluid Sci.* **12**, 190–196.

Williamson, C. & Govardhan, R. 2004 Vortex-induced vibrations. *Annu. Rev. Fluid Mech.* **36**, 413–455.